IEEE ROBOTICS AND AUTOMATION LETTERS. PREPRINT VERSION. ACCEPTED NOVEMBER, 2022

A Novel Metamorphic Foot Mechanism with Toe Joints based on Spring-loaded Linkages

Jianwei Sun, Zhenyu Wang, Meiling Zhang, Songyu Zhang, Zhihui Qian, and Jinkui Chu

***Abstract*—The toe joints play an important role in human walking and running movement patterns. In this paper, we propose a design method for metamorphic foot structures based on spring-loaded linkages to realize metatarsal-toe switching by using the self-recovery and self-stabilization properties of the spring-loaded linkages. We constrain the degrees of freedom (DOFs) of the foot mechanism by using the singular position characteristic of the four-bar mechanism to compensate for the lack of rigidity when the foot mechanism is in the toe line state. In addition, the structural parameters are calculated based on the static analysis method, and the validity of the design method is verified by simulation using Adams software. Finally, the compliance of the metatarsal state and the stability of the toe line state are demonstrated by physical prototyping and experiments. The results show that the novel metamorphic foot mechanism provides a uniform solution to cope with both walking and running movement modes.**

***Index Terms*—Compliant joints and mechanisms, mechanism design, metamorphic mechanism, metatarsal-toe switching, spring-loaded linkage.**

I. INTRODUCTION

In the last few years, a variety of structures of humanoid robots have been developed to meet the needs of engineering projects, sports training, etc. Starting from the development of the first humanoid robots by Hirose and Ogawa et al. [1], robots have gradually gained better balance and adaptability. Currently, most humanoid robots use rigid flat mechanical feet with elastic material as the base [2]. These foot structures are better able to walk on relatively flat ground, but the attitude control of the mechanical feet is usually achieved by motors to ensure that the robot's walking is stable, which reduces the smoothness and adaptability of humanoid robots.

To solve the problems of inadequate adaptability and the dependence on the control framework of the existing foot mechanism, we make further considerations in terms of the structural composition of the human foot and its related functions. As the only part in contact with the ground, the precise structure of the human foot achieves the unity of support, stability and compliance. The toe joint, which is located in it, plays an important role in foot movement. Additionally, changes in its flexion and extension characteristics have an important impact on the smoothness of running and walking, especially on the smoothness of the metatarsal gait cycle and the stability of the toe gait on the ground [3]. As shown in Fig. 1, when the human body is walking, the muscle tissue in the toe joint is in a relaxed state, which provides the high compliance required for toe flexion to achieve smooth walking in the metatarsal state. When the human body is running at a high speed, to increase the running speed, usually toes touch the ground to reduce the contact area to improve stamping efficiency [4]. The force locking of the toe also plays an important role in it.

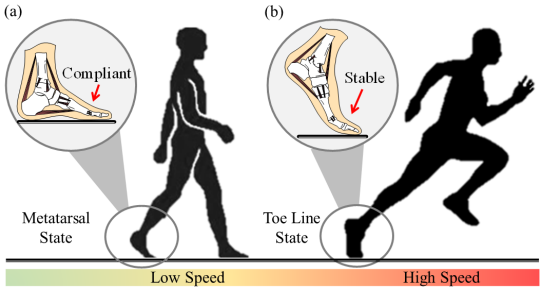

Fig. 1. Two modes of human movement. (a) Walking. (b) Fast running.

To improve walking fluency in the metatarsal state, the literature [5], [6] proposed a rigid foot mechanism with a three-stage structure and a toe deployment method based on a parallel mechanism from an adaptive perspective. The addition of such rigid members improved the stiffness and stability of the foot mechanism to a certain extent, but the compliance of the toe joint was not fully exploited. To highlight the role played by the toe during metatarsal walking, researchers, such as Zhu et al., arranged springs at the toe of the foot mechanism and used the arrangement of elastic members to improve the self-adaptability of the toe structure [7]. Choi et al. proposed a new foot mechanism using steel plate springs and rubber balls in a series to achieve a variable stiffness toe mechanism, which improved the adaptability to

Manuscript received July 28, 2022; Revised September 19, 2022; Accepted November 4, 2022.This paper was recommended for publication by Editor Clement Gosselin upon evaluation of the Associate Editor and Reviewers' comments. This work was supported by National Natural Science Foundation of China (no. 52275006) and Jilin Science and Technology Innovation and Entrepreneurship Excellence Project (20220508140RC). *(Corresponding author: Meiling Zhang)*.

J. Sun is with the School of Mechanical Engineering, Changchun University of Technology, Changchun 130012, China, and also with the Key Laboratory of Bionic Engineering, Jilin University, Changchun 130012, China.(e-mail: avensun@tom.com).

Z. Wang and S. Zhang are with School of Mechanical Engineering, Changchun University of Technology, Changchun 130012, China.(e-mail: wangzy98@tom.com; 815730432@qq.com).

M. Zhang is with School of Materials Science and Engineering, Changchun University of Technology, Changchun 130012, China. (e-mail: Zhangml@hrbeu.edu.cn).

Z. Qian is with the Key Laboratory of Bionic Engineering, Jilin University, Changchun 130012, China.(e-mail: zhqian@jlu.edu.cn).

J. Chu is with School of Mechanical Engineering, Dalian University of Technology, Dalian 116024, China.(e-mail: chujk@dlut.edu.cn).

Digital Object Identifier (DOI): see top of this page.

complex terrain [8]. The emergence of these two structures implied that maintaining the passive compliance of the toe joint contributed to fluidity during metatarsal walking. However, such toes with passive compliance were usually connected to the rear foot using coupled joints or flexible materials. This structure had the advantage of high compliance, but it also had the same drawback of poor stability and weak self-recovery caused by the release of DOFs of the flexible material. The "spring-loaded linkage" structure, which consists of rigid linkages and elastic members, has the trajectory stability of a linkage mechanism and also incorporates the self-recovery characteristics of springs and the force balance caused by internal stress. From the functional aspect, the hybrid rigidity and flexibility of this structure are functionally similar to the properties of the joint-ligament structure. Therefore, by introducing the spring-loaded linkages into the toe's design to achieve the human foot function, the self-recovery and stability needs of the toe structure can be ensured. Its self-stabilizing capacity is also employed to increase stability while walking and standing to prevent falling as a result of insufficient rigidity. Regarding self-recovery and multiple stability, spring-loaded linkages have attracted attention recently. For example, Woodward et al [9] and Li et al [10] used a spring linkage to form a diamond-shaped bouncing structure to complete the bouncing action of the robot with the help of its self-recovery property. Sangamesh et al [11] proposed a method to achieve static equilibrium of the linkage structure using a modified spring arrangement, which exhibits the multi-stability characteristics of the spring linkage structure. Unlike the toed foot structure using flexible materials [12], [13], to focus on features such as passive compliance and flexibility, it instead causes the defects of insufficient structural rigidity and weak self-recovery. The spring-loaded linkage benefits from its structural composition and has multi-stability characteristics while ensuring the self-recovery of the structure.

However, to more fully reproduce the unique functionality of the toe in the human foot, the toe line state of the human body under high-speed running should also be reflected in the mechanical function. In the running state, the toe joint provides toe flexion stability to meet the mechanical requirements of the human body when the toes touch the ground [4]. Therefore, the combination of two motion modes, adaptive walking in the metatarsal state and locked running in the toe line state can greatly improve the adaptability of the foot structure for a variety of operating conditions and reduce the difficulty of developing the control framework. To unify these two modes of motion, we incorporate the concept of metamorphic mechanisms into the existing structure. The metamorphic mechanism has the property of changing the function of the mechanism by changing the DOFs without changing the number of members, which is highly flexible. Therefore, the metamorphic mechanism can change its topology to achieve the ability to switch motion modes, which is positive theoretical support for the combination of two motion states of the foot structure. Benefiting from its structural properties, the "one mechanism, many functions" feature of the metamorphic mechanism has been widely used in the field of robotics for different work requirements [14]. To highlight the reconfigurability of the metamorphic mechanism. Dai et al. proposed a new palm structure with reconfigurable properties based on the metamorphic mechanism [15]. The flexibility and adaptability of the metamorphic mechanism were highlighted in the literature [16], where researchers built a parallel leg structure for a walking robot using the metamorphic mechanism's transformable degrees of freedom (DOF). In summary, combining the reconfigurable characteristics of the metamorphic mechanism with the self-recovery and self-stabilization advantages of the spring-loaded linkages enables the footed robot to have two motion modes, including adaptive walking in the metatarsal state and locked running in the toe line state, which can greatly enhance the robot's adaptability to a variety of terrains.

In this paper, a toe joint structure with metamorphic characteristics based on spring-loaded linkages is given, which has the flexibility property brought by the release of DOFs in the metatarsal state and the stability property brought by the locking structure in the toe line state. The spring-loaded linkages with metamorphic features can function in multiple topologies, enabling the integration of multiple motion states of the foot structure without affecting the smoothness of motion. This unique toe structure provides a unified solution for the foot mechanism to cope with both walking and running motion modes.

II. Proposed Configuration

A. Toe Joint Structure Selection

Considering that a humanoid robot needs to have a smooth gait during walking and provide rigid support when high-speed movement is required, the role of the toe joint in the human foot should be fully reflected. Easy deformable, self-recoverable designs are essential, and spring-loaded linkages significantly contribute to this need [17]. The constructed spring-loaded linkage is shown in Fig. 2.

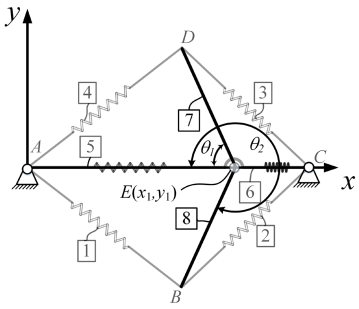

Fig. 2. Schematic diagram of the single steady-state of the spring-loaded linkage.

The structure consists of 5 nodes and 8 members. The members AB, BC, CD, AD, AE, and CE are tension ropes, and the members BE and DE are compression bars. On this basis, the rod BE and DE are arranged at node E with a rotational pair symmetrical with respect to the *x*-axis, and node E can move along the *x*-axis within the length of the

member AC. The members AE and CE are labeled as member 5 and member 6, respectively, and their lengths change with the movement of node E on AC. The sketch of the structure is shown in Fig. 2, the coordinates of node E are defined as (x_1, y_1), and the angles of member 7 and member 8 with the x-axis are θ_1 and θ_2, respectively. To ensure the force stability of the structure after the change, the tension cables 1, 2, 3, and 4 are replaced with light springs, and the light springs are arranged at AE and CE to ensure the force balance effect of node E after the movement in the x-direction. At this time, the structure has the following geometric relations:

$$\begin{cases} l_1 = l_4 \\ l_2 = l_3 \\ l_7 = l_8 = \dfrac{l_{AC}}{2} \\ l_5 + l_6 = l_7 + l_8 = l_{AC} \end{cases} \tag{1}$$

In the Cartesian coordinate system, the position of a component can be represented as $q = [x_i \ y_i \ \alpha_i]$. If coordinate of the nodes n_M is (x_M, y_M), then the node n_N associated with it can be expressed as:

$$n_N = \begin{bmatrix} x_M \\ y_M \end{bmatrix} + L_{MN} \begin{bmatrix} \cos\alpha_{MN} \\ \sin\alpha_{MN} \end{bmatrix} \tag{2}$$

Where L_{MN} is the distance from node M to node N. Thus, the coordinates of the structure node i (i =A, B, ... , E) shown in Fig. 2 are defined as n_i, and from the geometric relations it follows that:

$$\begin{aligned} &n_A = \begin{pmatrix} 0 \\ 0 \end{pmatrix};\ n_C = \begin{pmatrix} l_{AC} \\ 0 \end{pmatrix};\ n_E = \begin{pmatrix} x_1 \\ y_1 \end{pmatrix} \\ &n_B = \begin{pmatrix} x_1 \\ y_1 \end{pmatrix} - l_7 \begin{pmatrix} \cos\theta_1 \\ \sin\theta_1 \end{pmatrix};\ n_D = \begin{pmatrix} x_1 \\ y_1 \end{pmatrix} - l_8 \begin{pmatrix} \cos\theta_2 \\ \sin\theta_2 \end{pmatrix} \end{aligned} \tag{3}$$

This gives the length l of each elastic member:

$$\begin{aligned} l_1 &= n_B - n_A = (x_1, y_1)^T - l_7(\cos\theta_1, \sin\theta_1)^T \\ l_2 &= n_C - n_B = (l_{AC} - x_1, -y_1)^T + l_7(\cos\theta_1, \sin\theta_1)^T \\ l_3 &= n_D - n_C = (x_1 - l_{AC}, y_1)^T - l_8(\cos\theta_2, \sin\theta_2)^T \\ l_4 &= n_A - n_D = (-x_1, -y_1)^T + l_8(\cos\theta_2, \sin\theta_2)^T \\ l_5 &= n_E - n_A = (x_1, y_1)^T \\ l_6 &= n_C - n_E = (l_{AC} - x_1, -y_1)^T \end{aligned} \tag{4}$$

B. Mechanical Design

Based on the consideration that the toe joint motion pattern corresponds to different functionalities and the characteristics of the metamorphic mechanism change DOFs, it is designed as a 1-DOF structure with passive compliance in the metatarsal state and a 0-DOF structure with self-locking stability in the toe line state. The low friction characteristic of the slider provides a structural guarantee for the support of the metamorphic mechanism, based on which the topology is constructed by using the spring-loaded unit to meet the structural compliance design requirements of the toe joint. To improve the adaptability of the foot mechanism, we extend the previously studied adaptive foot structure [18] behind the existing toe structure.

When the foot switches to the toe line state according to the topological characteristics of the metamorphic mechanism, the stability of the rear foot should be ensured under downward pressure and certain torque to meet the efficient execution of the running action [19]. When a large external load is applied to a spring structure with a symmetrical arrangement, it will typically only be able to achieve its multi-stability characteristics under the influence of internal equilibrium, and this does not meet the requirements for pressure stability of the toe during running. Thus, the stability in the toe line state becomes an important issue to consider when designing the structure. To solve this problem, we add a four-bar mechanism outside the toe joint of the foot-type structure and use its singular position characteristic to achieve toe locking in the running state, and the structure diagram is shown in Fig. 3(a). The mechanism is actively locked when three of the four nodes in the four-bar mechanism are in a straight line position [20]. The inclusion of the four-bar mechanism enables the toe structure to complete locking while reducing the inclusion of other complex locking structures, thus reducing the structural complexity and the adverse effects of weight on the robot when walking and running. As shown in Fig. 3(b), the linkage structure at the toe joint is topologically transformed by translating the slider, and the rear foot is turned at a certain angle under the joint action of the spring and the connecting rod. When the slider moves to the end state, the four-bar mechanism composed of AD, AC, BC, and BD is in the singular position, as shown in Fig. 3(c). At this time, node D in connecting rod AD is located below the central axis MN, the position of slider B and connecting rod BE is locked, and this locks the rear foot to achieve the toe line state's pressure stability.

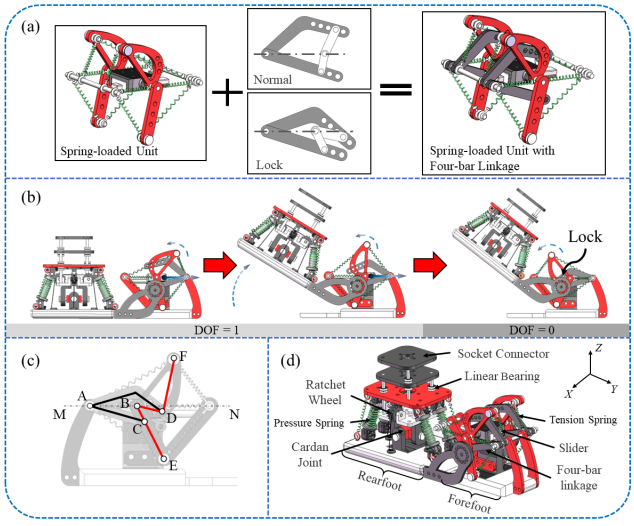

Fig. 3. Functional design of the foot structure. (a) Structural diagram of the spring-loaded unit. (b) Schematic diagram of metatarsal-toe switching. (c) Self-locking schematic diagram of the four-bar mechanism, where the black line segment is the four-bar structure and the red line segment is the spring-loaded linkage. (d) Isometric view of the foot structure.

When the foot structure is applied to a metatarsal walking situation, a complete gait cycle begins with a heel strike (HS), when multiple springs present at the toe joints and ankle joints are compressed during the heel strike. The compression of the four compression springs in the rearfoot ankle joint reaches its

peak when the foot flat phase (FF) is reached under the action of body pressure F_1. As the gait progresses, the heel-off phase (HO) is reached when the rearfoot leaves the ground under the combined action of the calf and compression springs in the form of force F_2. During this process, multiple springs are released at the ankle joint, generating a reaction force to facilitate the overturning action. As the rearfoot flips back to equilibrium, the elongated tension spring in the toe begins to contract, besides the toe stirrups off under tension to reach the toe-off phase (TO). An illustration of the gait cycle is shown in Fig. 4.

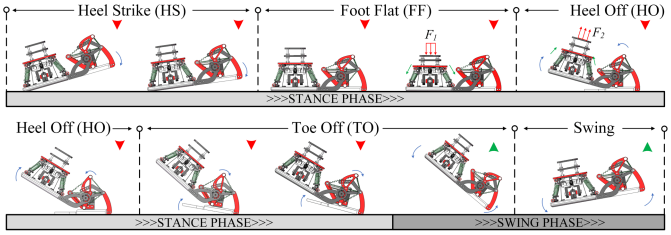

Fig. 4. Foot structure metatarsal walking gait cycle, including two states of a stance phase and a swing phase. There are four key points in the contact phase: HS, FF, HO, and TO. Red downward arrows indicate heel or toe contact with the ground, and green upward arrows indicate heel or toe separation from the ground.

III. Mathematical Analysis

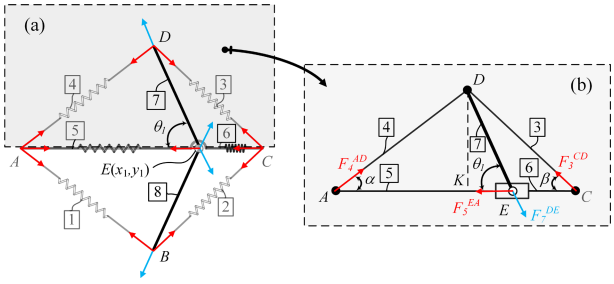

Fig. 5. Mechanical analysis diagram. Where the red arrows are the forces exerted by the elastic members and the blue arrows are the forces exerted by the rigid bars.

The force at each node of the structure is depicted in Fig. 5(a) when node E is situated in the right half of AC. The structure is divided along AC in Fig. 5(b) to make the analysis procedure simpler because the structure is symmetric about AC. Further, to ensure that the DOF does not change as a result, the node E can be equated to a slider structure in Fig. 5(b). Define $\angle DAC = \alpha$; $\angle DCA = \beta$, and draw the auxiliary line DK perpendicular to AC with node D as the origin downward. From the geometric relationship:

$$\alpha = \arctan\frac{DK}{AK} = \arctan\frac{l_7 \sin\theta_1}{x_1 - l_7\cos\theta_1}$$
$$\beta = \arctan\frac{DK}{CK} = \arctan\frac{l_7 \sin\theta_1}{l_{AC} - x_1 + l_7\cos\theta_1} \quad (5)$$
$$x_1 = \frac{1}{2}l_{AC} + l_7\cos\theta_1$$

Define the forces on the elastic members 3, 4, 5 in the structure shown in Fig. 5(b) as $F_3^{CD}, F_4^{AD}, F_5^{EA}$, respectively, and the forces on the rigid rod 7 as F_7^{DE}. From the mechanical relations it follows that:

$$\sum F_A = \sum M_A = \sum M_D = 0 \quad (6)$$

To ensure that the structure matches the motion characteristics of the human, the length of the member AC is set at l_{AC} =72mm, which in turn leads to $l_7 = l_8$ =36mm from the geometric relationship by (1). The angle between member 7 and the x-axis in the steady state of the structure is $\theta_1 = 60°$. The literature [7] gives the force that drives the toe to flex when the toe is stirred off as about 10 N. Therefore, in this paper, the driving force F_5^{EA} at node E along the AC direction is set to 10 N, i.e., $F_7^{DE} = F_5^{EA} \cdot \cos\theta_1 = 5\text{N}$. From (5) and (6) each structural parameter shown in Table 1 can be obtained.

TABLE I. STRUCTURAL PARAMETERS

Parameter	Value	Parameter	Value
α_1	43.373°	l_3	49.930mm
β_1	38.639°	l_4	45.398mm
x_1	51.06mm	l_6	20.740mm
y_1	0	F_3^{CD}	12.802N
l_{DK}	31.177mm	F_4^{AD}	13.757N

TABLE II. STIFFNESS COEFFICIENT OF ELASTIC MEMBERS

Member	Stiffness	Member	Stiffness
l_1	4.101N/mm	l_4	3.621N/mm
l_2	3.621N/mm	l_5	0.333N/mm
l_3	4.101N/mm	l_6	0.333N/mm

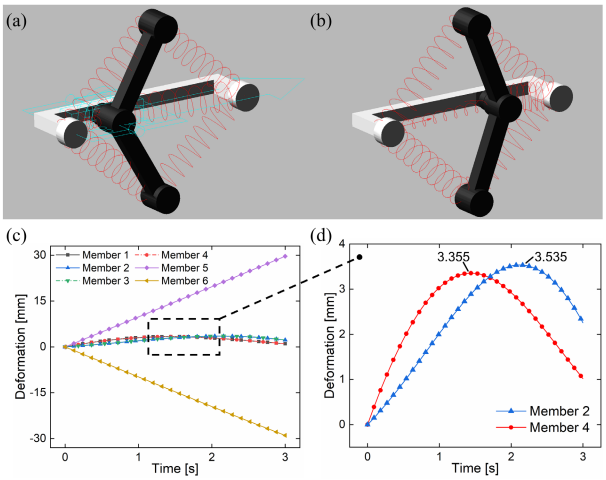

Fig. 6. ADAMS simulation results of spring-loaded linkage. (a) Steady state I. (b) Steady state II. (c) Length variation of elastic members. (d) Length variation and peak value of elastic members 2,4.

According to the parameters shown in Table 1, the structure is simulated using ADAMS analysis software, setting a gravity-free environment, no micro-minimal variation in the rod, and a constant force of 10N applied at the x-axis node. To deform the spring-loaded linkage structure deformed from the state shown in Fig. 6(a) to the structure shown in Fig. 6(b). From Fig. 6(c), 6(d), the maximum deformation variables of the elastic members 2,4 are: $\Delta l_2 = 3.535\text{mm}$, $\Delta l_4 = 3.355\text{mm}$. Combined with the data in Table 1 and Hooke's law shown in (7) can be calculated for each elastic member stiffness coefficient as shown in Table 2. From the calculation results, it can be noted that there are differences in the stiffness coefficients of springs l_2 and l_4, which help to balance the

applied main forces during toe joint bending and facilitate the construction of the solid prototype by referring to their proportional relationships.

$$k = \frac{F}{\Delta l} \tag{7}$$

IV. Experiment Validation

A. Metatarsal Walking Test

The three-dimensional model of the metatarsal walking test bench is shown in Fig. 7. The main execution unit of the walking test bench consists of three rods that constitute the crank-link mechanism and the profile sliding kit. The specific working principle is as follows: the regulated power supply (MP5050D) provides a stable voltage of 12 V, and then the DC motor pulse control board (YF-31) controls the DC high-torque motor to provide torque for the positive output of the active pendulum L_1 in the clockwise direction. The sliding kit (V-Slot) placed on the profile frame reduces the friction of the traveling actuator moving in the *y*-axis direction and limits the *x*-axis and *z*-axis errors that may affect the experimental results.

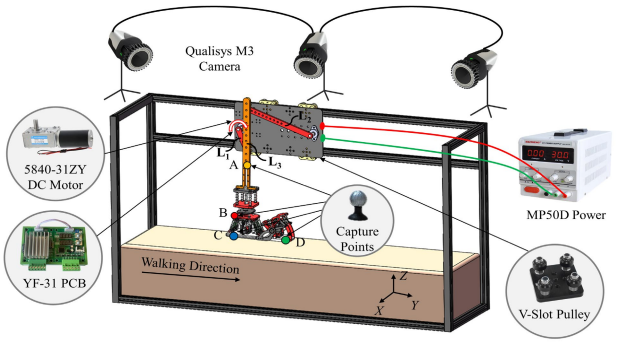

Fig. 7. The structural diagram of the experimental bench for the metatarsal walking experiment. The arrangement of 3D capture nodes A~D is also shown in the figure.

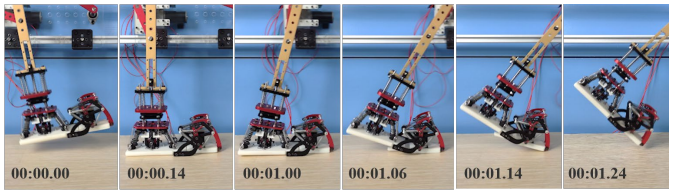

Fig. 8. The walking experimental gait diagram, the gait cycle starts from the heel strike to the end of the toe off phase, with a total time of 1.24s and a step frequency of 96 steps/min.

When the foot mechanism travels positively on the *y*-axis, the active rod L_1 rotates clockwise under the action of the motor, driving rods L_2 and L_3 to complete the cycle swing. The movement of the ankle part in the *z*-direction during walking is achieved by adding a buffer consisting of a compression spring at the part below rod L_3 where it meets the foot mechanism. The 3D capture device (Miqus M3, Max sampling rate 650 Hz, Qualisys Co.) is used to read the data in the gait cycle to capture the motion trajectory of the foot mechanism in the spatial state in real-time.

The experimental process is shown in Fig. 8. The entire gait cycle from heel strike to toe-off was completed under the regulated power supply. At this time, the compression of the spring at the ankle joint of the rear foot and the forward movement of the whole joint can be seen, and at 1.00 s, the center of gravity moves to the position of the forefoot, and the spring at the toe joint begins to deform. At 1.06 s, the rear foot is raised, when the compression spring at the ankle joint is released, which in turn leads to the deformation of the elastic member at the toe. The whole foot structure in this gait phase is completed with an accelerated gait. During this gait phase, the entire foot structure completes the toe-off phase from 1.06 s to 1.24 s in an accelerated manner. The accelerated motion during the toe-off phase demonstrates the smoothness and compliance of the toe joints.

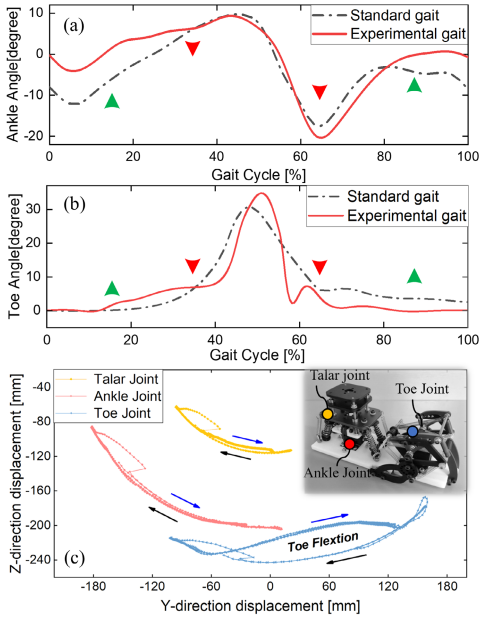

Fig. 9. The experimental results of metatarsal walking. (a) Variation in ankle joint angle. (b) Variation in toe angle. (c) Foot structure of the talar joint, ankle joint, and toe joint's workspace. The red downward arrows in Fig. 9(a) and (b) indicate that the heel or toe is in contact with the ground, and the green upward arrows indicate that the heel or toe is separated from the ground.

By using the 3D motion capture system for analysis of the walking gait, we arrange motion capture nodes A, B, C, and D at the walking frame, talar joint, ankle joint, and toe joint, as shown in Fig. 7, and analyze the data of the foot structure gait cycle at a 600 Hz sampling rate to extract each key gait of a single cycle. Fig. 9(a) and 9(b) analyze the angular changes of the ankle and toes during each phase of the gait cycle, respectively, and compare them with the standardized data from the literature [3], [21]. At the beginning of the gait phase, there is a small change in the angle between the ankle joint and the toe under gravity, and the heel is grounded when reaching 40% of the gait. When the metatarsal gait cycle is in the 40% ~ 65% phase, the foot mechanism achieves 10° ~ 20° dorsiflexion motion of the ankle joint and 0 ~ 35° toe flexion motion of the toes in a short period. This process corresponds to the heel-off and the toe-off phases of the gait cycle, where the foot structure is rapidly separated from the ground by the combined action of the elastic member and the linkage mechanism. In the latter part of the gait cycle, the ankle joint

angle changes linearly, and the toe gradually returns to the rear foot parallel position and enters the swing phase. Fig. 9(c) extracts the three important joint parts of the foot separately and plots the workspace of each marker point by capturing the metatarsal gait cycles occurring in the *o-yz* plane, with the blue arrows in the figure showing the spatial trajectories delineated at the nodes of the forward walking process and the black arrows showing the spatial point connections delineated at the walking recovery segment. The spatial points of the toe joint in the blue line can be seen in the overlapping sampling states of several gait cycles, and the spatial trajectories of the foot structure in the forward walking process and the walking recovery segment are not identical. The difference point is that the high flexibility at the toe joint provides a smoother walking state for the gait cycle, i.e., the passive toe flexion motion of the toe structure occurs in the curve's no overlap phase, and this feature is also demonstrated in Fig. 8.

B. Toe Line Stability Test

To meet the toe line state of the rear foot in the fast running state to maintain stability and high efficiency of force transfer, the toe line state's stability should be verified. As a result, we use high-precision distance and pressure sensors to examine the relationship between rear foot torque and rotation angle. The test bench is shown in Fig. 10(a). At this time, the toe joint's four-bar mechanism's node C is in the singular position below the horizontal line MN, and the rear foot is locked. The contact position of the pressure probe is the center of the rear foot, i.e., the position of the ankle joint, and the pressure is applied in this direction to analogize the force state of the human foot in the fast-running state. Referring to the force state of the toe in the running state provided in the literature [4], the force application interval given in the experiment was 0-50 N. Fig. 10(b) ~ Fig.10(f) shows six sets of experimental data measured in steps of 10N.

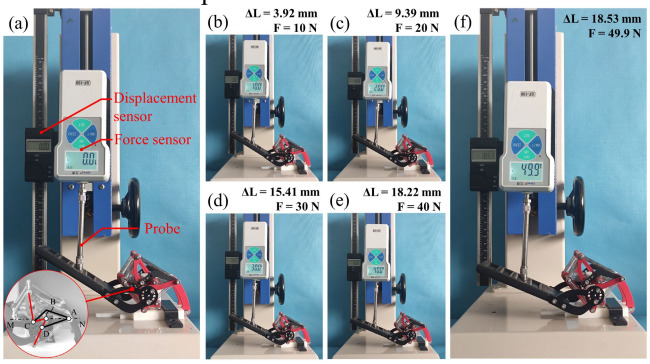

Fig. 10. Toe line stability experiment force test diagram, apply 0 ~ 50N vertical force, used to prove the role played by the four-bar mechanism in maintaining stability.

By collecting and analyzing the data and calculating the torque in combination with $M = F \cdot L$, the torque versus torsion angle curve is plotted as shown in Fig. 11. It can be seen that when the moment is 0~4Nm, the change of the turning angle is more obvious due to the structural assembly gap and the low stiffness of the elastic member as the applied load continues to increase. The curve tends to be smooth when the torque is further increased to the range of 4~6.5Nm, which shows that the four-bar mechanism plays a role in maintaining the stability after the state switching.

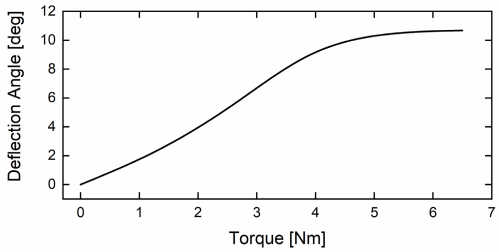

Fig. 11. Torque versus angle of rotation, and smoothing out during pressure application of 5Nm~6.5Nm.

C. Two-state Vertical Force Test

To ensure that the foot structure has the same force trend compared to the human body in both metatarsal and toe walking motion states to ensure the correct mechanical performance for the user, the built Jansen linkage [22] based vertical force test bench is shown in Fig. 12(a). On either side of the walking test bench, two cantilever beam load cells (YZC-1B) were placed symmetrically, and the HX711 conversion chip in conjunction with the XL-F3M controller's communication serial connection was used to attach to the computer for data collecting.

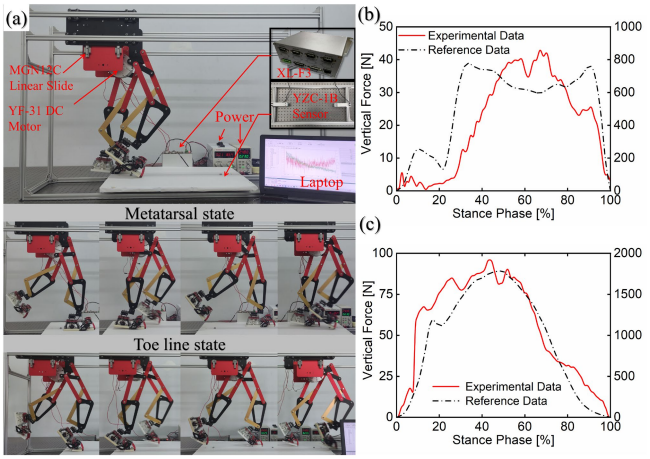

Fig. 12. Bipedal pressure test bench based on Jansen linkage. The lower part of Fig. 12(a) shows the experimental process in the metatarsal and toe line states respectively. Fig.12(b), Fig.12(c) record the mechanical data of the metatarsal and toe line states respectively, and the ratio of experimental data to reference data is 1:20.

Using the XL-Center controller software to decouple the electrical signals transmitted by the HX711 chip, the vertical pressure distribution data relative to the ground during the gait cycle were extracted and compared with the vertical reaction force data of a human wearing a marketed ankle-foot prosthesis (1S90, Ottobock) in the walking state [7] and the running state data in the literature [23], respectively. Fig.12(b) shows the comparison of the forces in the walking state, it can be seen that in the first half of the experimental data compared to the literature data in the dynamic equilibrium of the elastic member has more peaks, with a certain buffering capacity. The vertical force rises more gently, and the mechanical properties are more compact when reaching the highest point. Fig. 12(c) shows a comparison of the vertical force when the foot structure is locked in the toe line state in the running

condition, from which it is easy to see that the experimental data and the reference data have similarities in the trend, compared with the slope of the experimental data is more obvious, and the force is significantly greater than the walking state shown in Fig. 12(b), which can better meet the mechanical requirements of the running pedal state.

D. Foot Structure Walking Comparison Test

To compare the functional differences between the foot structure proposed in this paper and other dominant foot structures, each of the three foot structures shown in Fig. 13(a) was tested using the walking test bench built in Experiment C. Among them, the prototype of the Normal-toe Foot was taken from the literature [7], and the No-toe Foot was made with the foot structure introduced in the literature [24]. In addition, to exclude the influence of material and prototype size on hardness and ground friction, all three foot structures are made of PLA as the base plate and have the same dimensional parameters.

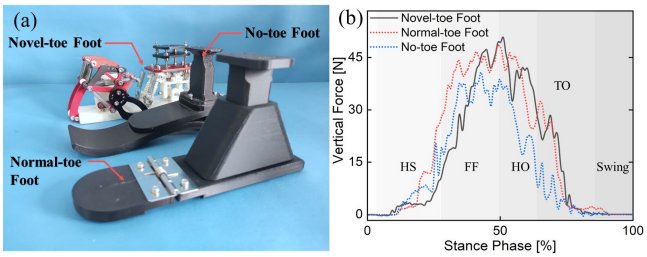

Fig. 13 Foot structure walking comparison experimental diagram.

The experimental data are shown in Fig. 13(b). From the image, it can be seen that in the HS segment, there is a larger curve step between Normal-toe Foot and No-toe Foot. And this feature continues to extend to the FF segment. The difference starts to be gradually obvious in the FF segment, and No-toe Foot has an advantage in stability because of the existence of curved transition in its heel, which makes the force change of touchdown less than the flat foot structure. In addition, the location of peak values of the two toe-structured feet overlaps, with the difference that the Novel-toe Foot is more gentle in the rising phase of the curve and has better compliance. The peak of the two toe-structured feet occurred in the HO interval, and the peak of the Novel-toe Foot in the first half of the interval was 51.4N, which was higher than the 48.7N of the Normal-toe Foot and had better mechanical properties. In the latter half of the interval there is a downward fluctuation with a span of 21N and then returns to the normal position, in which the self-recovery effect of the elastic member is reflected. It is worth noting that although the No-toe Foot also has extreme points in the HO interval, its highest peak value is located in the FF interval, which indicates that the toe structure acts as a support during the transfer of the force point from the heel to the forefoot. In the TO phase, the No-toe foot has only one torsional spring, so it has a shorter stomp-off duration and moves more quickly to the next gait cycle. In contrast, the Novel-toe Foot has more elastic components, resulting in more fluctuations during the stirrups, thus extending the gait cycle duration to a small extent.

V. Discussion

We design, build and test a new foot structure with a metatarsal-toe switch in this paper, which combines the suppleness of the metatarsal state with the stability of the toe line state in a single structure that can switch modes for varied movement requirements. The tests in Chapter 4 demonstrate the foot structure's functionality and capabilities, meeting the majority of the stated aims and design requirements outlined in Chapter 1.

The foot structure tends to move with joint angles similar to those of the human body, as demonstrated in the tests conducted in Experiment A for joint angles. Unfortunately, because of the differences between the test rig and human unconstrained walking, it was not possible to verify that the same gait could be accomplished during unconstrained walking in an undefined environment, only to demonstrate that it has the same compliant toe flexion capability as other footed. Further, to improve the performance of the foot structure in a relatively realistic environment, we built an experimental bench based on the Jansen linkage mechanism to imitate the motion state of human lower limbs, with sensors collecting and recording the vertical reaction force to verify its mechanical performance. By unifying the numerical scale, it can be found that in Fig. 12(b), by calculating the rising slope, it can be seen that $k_{\mathrm{Ref}}=2.7>k_{\mathrm{Exp}}=1.4$, i. e. the novel foot structure has a smoother touchdown process. It exhibits the same phenomenon as the Normal-toe Foot comparison experiment shown in Fig. 13(b), which demonstrates that the mechanical characteristics of the foot structure are primarily reflected in the first half of the gait cycle. The average value of vertical force conversion in the range of 40% to 80% of the gait cycle is 25% higher than the reference data, while its peak value in the 80% to 100% phase is 28% lower than the reference data. The compliance of the toe joint is reflected in this process.

It is worth noting that the foot structure is not only able to meet the walking needs, but more importantly, it can obtain the support capacity for a high-speed running state by switching the state of the mechanical structure without changing the number of components. Experiment B was conducted by applying pressure to the locked toe joint and processing the data into torque to observe the role played by the four-bar mechanism in maintaining stability. During the experiment, we noticed that the stiffness and mounting accuracy could not be unified because the existing foot structure was composed of a mixture of 3D printed parts and metal parts, which led to an error rotation of about 10° still existing during the downward pressure after locking, but the angle change tended to stabilize with the increase of torque in the second half of Fig. 11. In Fig. 12(c), the characteristics of the toe line state are also depicted. The force distribution in the running state essentially overlaps with that of the human body, but because of the flat design of the toe, which differs from that of the human body, the experimental data show a particularly prominent upward tendency, which in turn affects the stability.

In summary, compared with other mainstream foot structures [2], the foot structure proposed in this paper has a unique bistable design in terms of functionality, and no other toe joint structure with a similar function has been found. In the walking state, the passive toe flexion function and the self-recovery of the spring-loaded linkages are superior compared to the mainstream toed foot structures such as PANTOE [7] and AMP-Foot [25]. However, the load-bearing capacity under the current structural configuration is weaker than the mainstream structures mentioned above due to the limitations of the available prototype materials. This leads to bench-based mechanical experiments to verify the correlation of the curves only by normalization, which reduces the objectivity of the experimental results.

As a result, future research will integrate the segmented parts and strengthen the material to increase the rigidity of the structure and enable it to support greater weight to address the above-mentioned unresolved issues. Additionally, to establish active control for bistable switching of the toe joint, it will be coupled in series with the leg structure.

V. Conclusion

In this paper, through a systematic study of the function of toe joints of the human foot, a metamorphic foot structure based on the spring-loaded linkages that can realize metatarsal-toe switching is proposed. A four-bar mechanism is introduced into the spring-loaded linkage, and its singular position characteristic can be used to provide locking when the forefoot and the rear foot are at a certain angle to realize the locking of the toe in the toe line state and to improve the force stability in the high-speed running state. The foot structure has the compliant characteristics of the metatarsal state and the stable characteristics of the toe line state, which can realize smooth walking in the metatarsal walking state and high-speed running in the toe line state, providing a solution for different walking modes.

A walking test bench was built and a 3D motion capture system was used to experimentally verify the motion of each key part of the foot structure during the foot structure gait cycle, and a force test bench based on Jansen linkage was built to verify the mechanical properties of the foot structure during utilization. The results show that the foot structure can provide joint motion and mechanical properties with similar trends to the human body.

References

[1] M. Hirose and K. Ogawa, “Honda humanoid robots development,” *Philos. Trans. R. Soc. A Math. Phys. Eng. Sci*., vol. 365, no. 1850, pp. 11–19, 2007.

[2] P. Cherelle, G. Mathijssen, Q. Wang, B. Vanderborght, and D. Lefeber, “Advances in propulsive bionic feet and their actuation principles,” *Adv. Mech. Eng*., vol. 2014, 2014.

[3] E. C. Honert, G. Bastas, and K. E. Zelik, “Effect of toe joint stiffness and toe shape on walking biomechanics,” *Bioinspiration and Biomimetics*, vol. 13, no. 6, 2018.

[4] C. Rolian, D. E. Lieberman, J. Hamill, J. W. Scott, and W. Werbel, “Walking, running and the evolution of short toes in humans,” *J. Exp. Biol*., vol. 212, no. 5, pp. 713–721, 2009.

[5] K. Yamamoto, T. Sugihara, and Y. Nakamura, “Toe joint mechanism using parallel four-bar linkage enabling humanlike multiple support at toe pad and toe tip,” *Proc. 2007 7th IEEE-RAS Int. Conf. Humanoid Robot. HUMANOIDS 2007*, pp. 410–415, 2007.

[6] M. Russo, B. D. M. Chaparro-Rico, L. Pavone, G. Pasqua, and D. Cafolla, “A bioinspired humanoid foot mechanism,” *Appl. Sci*., vol. 11, no. 4, pp. 1–15, 2021.

[7] J. Zhu, Q. Wang, and L. Wang, “On the Design of a Powered Transtibial Prosthesis With Stiffness Adaptable Ankle and Toe Joints,” *IEEE Trans. Ind. Electron*., vol. 61, no. 9, pp. 4797–4807, Sep. 2014.

[8] W. Choi, G. A. Medrano-Cerda, D. G. Caldwell, and N. G. Tsagarakis, “Design of a variable compliant humanoid foot with a new toe mechanism,” *Proc. - IEEE Int. Conf. Robot. Autom*., vol. 2016-June, pp. 642–647, 2016.

[9] M. A. Woodward and M. Sitti, “MultiMo-Bat: A biologically inspired integrated jumping-gliding robot,” *Int. J. Rob. Res*., vol. 33, no. 12, pp. 1511–1529, 2014.

[10] X. Yin, J. Yan, S. Wen, and J. Zhang, “Spring-linkage integrated mechanism design for jumping robots,” *Rob. Auton. Syst*., p. 104268, Sep. 2022.

[11] S. R. Deepak and G. K. Ananthasuresh, “Perfect static balance of linkages by addition of springs but not auxiliary bodies,” *J. Mech. Robot*., vol. 4, no. 2, pp. 1–12, 2012.

[12] M. G. Catalano et al., “Adaptive Feet for Quadrupedal Walkers,” *IEEE Trans. Robot*., vol. 38, no. 1, pp. 302–316, 2022.

[13] C. Piazza et al., “Toward an adaptive foot for natural walking,” *IEEE-RAS Int. Conf. Humanoid Robot*., pp. 1204–1210, 2016.

[14] L. Zhang and J. S. Dai, “An overview of the development on reconfiguration of metamorphic mechanisms,” *Proc. 2009 ASME/IFToMM Int. Conf. Reconfigurable Mech. Robot. ReMAR 2009*, pp. 8–12, 2009.

[15] E. Emmanouil, G. Wei, and J. S. Dai, “Spherical trigonometry constrained kinematics for a dexterous robotic hand with an articulated palm,” *Robotica*, vol. 34, no. 12, pp. 2788–2805, 2016.

[16] Y. Xu, Z. Liang, and J. Liu, “A New Metamorphic Parallel Leg Mechanism with Reconfigurable Moving Platform,” *Math. Probl. Eng*., vol. 2020, 2020.

[17] G. Jung et al., “JumpRoACH : A Trajectory-Adjustable Integrated Jumping – Crawling Robot,” *IEEE/ASME Trans. Mechatronics*, vol. 24, no. 3, pp. 947–958, 2019.

[18] J. Sun, S. Zhang, Z. Wang, G. Song, M. Zhang, and J. Chu, “Design of a new foot structure based on the mast-type octahedral tensegrity structure,” *Mech. Mach. Theory*, vol. 177, no. July, p. 105016, 2022.

[19] D. R. Carrier and C. Cunningham, “The effect of foot posture on capacity to apply free moments to the ground: Implications for fighting performance in great apes,” *Biol. Open*, vol. 6, no. 2, pp. 269–277, 2017.

[20] M. Plooij, G. Mathijssen, P. Cherelle, D. Lefeber, and B. Vanderborght, “Lock your robot: A review of locking devices in robotics,” *IEEE Robot. Autom. Mag*., vol. 22, no. 1, pp. 106–117, 2015.

[21] J. Camargo, A. Ramanathan, W. Flanagan, and A. Young, “A comprehensive, open-source dataset of lower limb biomechanics in multiple conditions of stairs, ramps, and level-ground ambulation and transitions,” *J. Biomech*., vol. 119, p. 110320, 2021.

[22] S. Nansai, N. Rojas, M. Rajesh Elara, R. Sosa, and M. Iwase, “On a Jansen leg with multiple gait patterns for reconfigurable walking platforms,” *Adv. Mech. Eng*., vol. 7, no. 3, pp. 1–18, 2015.

[23] K. Bas, B. S. W, Z. Sjouke, Z. Wiebren, and B. Ida, “Comparison of vertical ground reaction forces during overground and treadmill running. A validation study,” *BMC Musculoskelet. Disord*., vol. 13, no. 1, p. 235, 2012.

[24] A. Agboola-Dobson, G. Wei, and L. Ren, “Biologically Inspired Design and Development of a Variable Stiffness Powered Ankle-Foot Prosthesis,” *J. Mech. Robot*., vol. 11, no. 4, pp. 1–15, 2019.

[25] P. Cherelle, K. Junius, V. Grosu, H. Cuypers, B. Vanderborght, and D. Lefeber, “The AMP-Foot 2.1 : actuator design , control and experiments with an amputee,” *Robotica*, no. September 2014, pp. 1347–1361, 2015.